

# Frequency Subspace Amplitude Flow for Phase Retrieval

Zhun Wei<sup>1</sup>, Wen Chen<sup>2,3</sup>, and Xudong Chen<sup>1</sup>

<sup>1</sup>*Department of Electrical and Computer Engineering, National University of Singapore, 4 Engineering Drive 3, 117583, Singapore*

<sup>2</sup>*Department of Electronic and Information Engineering, The Hong Kong Polytechnic University, Hong Kong, China*

<sup>3</sup>*The Hong Kong Polytechnic University Shenzhen Research Institute, 518057, China*

This research was supported by the National Research Foundation, Prime Minister's Office, Singapore under its Competitive Research Program (CRP Award No. NRF-CRP15-2015-03). The support from Shenzhen Science and Technology Innovation Commission (Basic Research Program) under Grant No. JCYJ20160531184426473 is also acknowledged.

**Abstract:** A novel approach, termed frequency subspace amplitude flow (FSAF), is proposed to reconstruct complex-valued signal from "phaseless" measurements. The proposed FSAF consists of two stages: The first stage approximates low-frequency coefficients of an unknown signal by spectral method, and the second stage refines the results by truncated conjugate gradient of amplitude-based nonconvex formulation. FSAF is easy to implement and applicable to natural images, where no additional constraint is needed. Extensive experiments with 1D signals, 2D images and natural images corroborate significant improvements by using the proposed FSAF method over the state of the art. Especially for sample complexity, FSAF pushes state-of-the-art for exactly reconstructing complex natural signals (with a size of  $n$ ) from  $3.2n$  to  $2.2n$  under Gaussian model, and from  $5n$  to  $3n$  under coherent diffraction pattern (CDP) model without increasing computational complexity. More importantly, the proposed method is highly flexible and can be easily adapted to the existing algorithms under different noise models.

**Index Terms:** Phase retrieval, frequency subspace, spectral method, coherent diffraction pattern.

## 1. Introduction

Phase retrieval (PR), which aims to reconstruct an unknown signal or image from phaseless measurements, is related with quadratic equations of the form:

$$y_i = |\mathbf{a}_i^H \mathbf{z}|^2, \quad i = 1, 2, \dots, m, \quad (1)$$

where  $m$  is the total number of measurements, superscript  $H$  denotes the Hermitian transpose,  $\mathbf{z}$  is a complex vector with the size of  $n \times 1$  to be recovered,  $\mathbf{a}_i$  is the  $i$ th measurement vector, and  $y_i$  is the  $i$ th magnitude-squared observation of the linear measurement of any complex vector  $\mathbf{z}$ . Algorithmic PR plays an important role in science and engineering, such as coherent diffraction imaging [1], [2], digital holographic microscopy [3], and optical encryption [4], [5], [6].

Due to the significance of PR problem, numerous algorithms have been developed. Alternating projection method, which was proposed by Gerchberg and Saxton (GS) [7], is most widely used. Later, Fienup has improved GS algorithm and proposed a hybrid input-output method (HIO) [8] by applying certain constraints. Over the years, numerous PR algorithms have been proposed based

on GS and HIO, such as difference map [11], guided HIO [12], and particle swarm optimization [13]. The major drawback of GS algorithm and its modified methods would be that it is very difficult to ensure the convergence theoretically due to the use of projections onto nonconvex constraint set [9], [10]. In addition, these methods combined with oversampling tend to return solutions that depend on an initial guess, which means that different runs return different solutions [14]. Thus, different random values are widely used in the initial step to obtain a better reconstruction result. In many cases, it is difficult to distinguish a better reconstruction result since one does not know the details of specimen under test.

Recently, some theoretically convergent algorithms have also been proposed. Among them, PhaseLift algorithm converts the non-convex problem into a convex one by using lift technique of semi-definite programming (SDP) [15]. However, this approach requires a lift of matrix and thus highly increases computational cost. A gradient descent scheme, i.e., Wirtinger flow (WF) algorithm, has later been reported and is demonstrated to allow exact recovery of the phase from magnitude measurements [16]. Recently, to reduce sample complexity and increase convergence rate of WF, improved algorithms have been proposed such as conjugate gradient Wirtinger flow (CGWF)[17], truncated Wirtinger flow (TWF) [18], truncated amplitude flow (TAF) [19], and stochastic truncated amplitude flow (STAF) [20]. Moreover, signal priors, such as sparsity or constraints, are incorporated into the algorithms [21], [22], [23].

In this paper, we propose a frequency subspace amplitude flow (FSAF) approach to reconstruct natural signals from “phaseless” measurements. The proposed FSAF consists of two stages: The first stage approximates low-frequency coefficients of an unknown signal by spectral method, and the second stage refines the results by truncated conjugate gradient of amplitude-based nonconvex formulation.

The motivation of the first stage of FSAF lies in the fact that, from the statistics [24], most information of natural images is concentrated in low spatial frequency bands. At the first stage, there are some well-known algorithms such as WF [16], TWF [18], TAF [19], and STAF [20], which focus on finding the approximation of a complex signal  $\mathbf{z}$  with a size of  $n \times 1$ . Instead, this paper finds the approximation of low-frequency coefficients  $\mathbf{c}$  of  $\mathbf{z}$  at the first stage, where  $\mathbf{c}$  is with a size of  $s \times 1$ . Since low spatial frequency bands can be represented by using only a few low-frequency coefficients, we have  $s \ll n$ , which means a significant reduction in the number of unknowns. Thus, the proposed FSAF is able to largely reduce sample complexity compared with other algorithms. The motivation for the second stage of FSAF is that, in previous algorithms with amplitude gradient such as TAF [19] and STAF [20], a gradient descent direction is used, which makes the methods easily take steps in the same direction as the earlier steps and consequently move zigzag to the solution. Instead, this paper adopts conjugate gradient of the amplitude-based objective function, which combines the derivative linearly with previous search directions, and move to the solution with fewer steps. Moreover, an adaptive optimized step size is used in FSAF instead of a constant step size in TAF [19].

*Notation:* We use bold uppercase and lowercase letters to represent matrices and vectors, respectively.  $\text{Re}(\cdot)$  represents real part of a complex valued number, and  $|\cdot|$  denotes absolute value of a real number or the modulus of a complex number. Furthermore, we use  $\|\cdot\|$  and  $\|\cdot\|_F$  to denote Euclidean norm and Frobenius norm, respectively. Finally,  $j = \sqrt{-1}$  is used to denote imaginary unit.

## 2. Algorithm: Frequency Subspace Amplitude Flow

To recover an unknown signal  $\mathbf{z}$  in (1), the following intensity-based objective function [16], [18]:

$$\min f_1(\mathbf{z}) = \frac{1}{2m} \sum_{i=1}^m (|\mathbf{a}_i^H \mathbf{z}|^2 - y_i)^2, \quad (2)$$

or the amplitude-based objective function [19], [20] is usually used

$$\min f_2(\mathbf{z}) = \frac{1}{2m} \sum_{i=1}^m (|\mathbf{a}_i^H \mathbf{z}| - \sqrt{y_i})^2. \quad (3)$$

### 2.1. Frequency Subspace Initialization

Let  $\mathbf{A}$  be the  $m \times n$  matrix whose  $i$ th row is  $\mathbf{a}_i^H$ , (1) can be easily transformed as  $\mathbf{y} = |\mathbf{A}\mathbf{z}|^2$  with the  $i$ th element in  $\mathbf{y}$  be  $y_i$ . In WF method [16], the initialization  $\mathbf{z}_0$  is calculated via a spectral method, i.e.,  $\mathbf{z}_0$  calculated as the leading eigenvector of  $\mathbf{A}^H \text{diag}(\mathbf{y})\mathbf{A}$  by power iteration method.

In the first stage of FSAF,  $\mathbf{z}_0$  is approximated by its the low-frequency coefficients  $\mathbf{c}_0$  by power iteration method with

$$\mathbf{z}_0 = \mathbf{f}_1 c_1 + \mathbf{f}_2 c_2 + \dots + \mathbf{f}_s c_s = \mathbf{F}_l \mathbf{c}_0. \quad (4)$$

Here,  $\mathbf{F}_l$  is low-frequency subspace matrix with the size of  $n \times s$ , and is composed by low-frequency Fourier bases as  $[\mathbf{f}_1, \mathbf{f}_2, \dots, \mathbf{f}_s]$ . Specifically, for one dimension (1D) case, element  $F_{g,h}$  in Fourier matrix  $\mathbf{F}$  is calculated as  $F_{g,h} = e^{(-2\pi j((g-1)(h-1)/n))}$ .  $[\mathbf{f}_1, \mathbf{f}_2, \dots, \mathbf{f}_s]$  is the low-frequency bases chosen from  $\mathbf{F}$ . In practice,  $\mathbf{F}_l \mathbf{c}_0$  can be easily calculated by using fast Fourier transform (FFT) by padding  $\mathbf{c}_0$  with zeros for high-frequency coefficients. The details of padding methods for both 1D and 2D cases will be discussed in numerical experiments.

In the power iteration method of FSAF, truncated intensity  $\mathbf{y}_t = \mathbf{y} \circ \gamma\{\mathbf{y} \leq \alpha^2 \phi\}$  [18] is used to approximate  $\mathbf{c}_0$ , where “ $\circ$ ” denotes Hadamard product. Here,  $\gamma$  is a logical matrix with element being 1 when the condition  $\mathbf{y} \leq \alpha^2 \phi$  is satisfied. If the condition is not satisfied, then the value is equal to zero.  $\phi$  is the mean value of  $\mathbf{y}$  and  $\alpha$  is a constant parameter around 2.5. The implementation procedure of initialization in the proposed FSAF method is to calculate the leading eigenvector of  $(\mathbf{A}\mathbf{F}_l)^H \text{diag}(\mathbf{y}_t)\mathbf{A}\mathbf{F}_l$  by power iteration method, and the details can be described as:

- Step 1) Let  $n = 1$ , randomly generate a frequency coefficient vector  $\mathbf{c}_0$ , and normalize it with  $\mathbf{c}_0 = \mathbf{c}_0 / \|\mathbf{c}_0\|_F$ .
- Step 2) Calculate  $\mathbf{c}'_0 = (\mathbf{A}\mathbf{F}_l)^H (\mathbf{y}_t \circ \mathbf{A}\mathbf{F}_l \mathbf{c}_0)$ . Here, the multiplication of  $\mathbf{F}_l^H$  or  $\mathbf{F}_l$  with a vector or matrix can be calculated by FFT or inverse fast Fourier transform (IFFT), respectively.
- Step 3) Update  $\mathbf{c}_0$  as  $\mathbf{c}_0 = \mathbf{c}'_0 / \|\mathbf{c}'_0\|_F$ .
- Step 4) If  $n = M_{ite}$  ( $M_{ite} = 20$  in this paper), stop the iteration and  $\mathbf{z}_0 = \sqrt{\phi} \mathbf{F}_l \mathbf{c}_0$ . Otherwise, let  $n = n + 1$ , and go to step 2).

### 2.2. Truncated conjugate gradient stage

In TAF [19], the second stage iteratively updates  $\mathbf{z}_{k+1}$  for  $k = 0, 1, 2, \dots$  by using the following equation:

$$\mathbf{z}_{k+1} = \mathbf{z}_k - \alpha_k \mathbf{d}_{tk}, \quad (5)$$

where stepsize  $\alpha_k$  is empirically chosen around 0.6 for TAF method. The search direction  $\mathbf{d}_{tk}$  is the truncated gradient of amplitude-based objective function [19]

$$\mathbf{d}_{tk} = \frac{1}{m} \sum_{i \in \beta_k} (\mathbf{a}_i^H \mathbf{z}_k - \sqrt{y_i} \frac{\mathbf{a}_i^H \mathbf{z}_k}{|\mathbf{a}_i^H \mathbf{z}_k|}) \mathbf{a}_i, \quad (6)$$

where  $\beta_k := \{1 \leq i \leq m \mid \frac{|\mathbf{a}_i^H \mathbf{z}_k|}{\sqrt{y_i}} \geq \frac{1}{1+\gamma_0}\}$  with a constant parameter  $\gamma_0$  around 0.7.

In the second stage of the proposed FSAF method, instead of directly using truncated derivative of amplitude-based objective function, Polak-Ribière-Polyak (PRP) direction [25] is used as the direction for updating  $\mathbf{z}_{k+1}$  in (5). Specifically,  $\mathbf{d}_{tk}$  in Eq. (5) is replaced by  $\mathbf{v}_k$ , where  $\mathbf{v}_k$  is calculated as follows: If  $k = 0$ , then  $\mathbf{v}_0 = \mathbf{d}_{t0}$ ; Otherwise [26],

$$\mathbf{v}_k = \mathbf{d}_{tk} - (\text{Re}[\mathbf{d}_{tk}^H \cdot (\mathbf{d}_{tk} - \mathbf{d}_{tk-1})] / \|\mathbf{d}_{tk-1}\|^2) \mathbf{v}_{k-1} \quad (7)$$

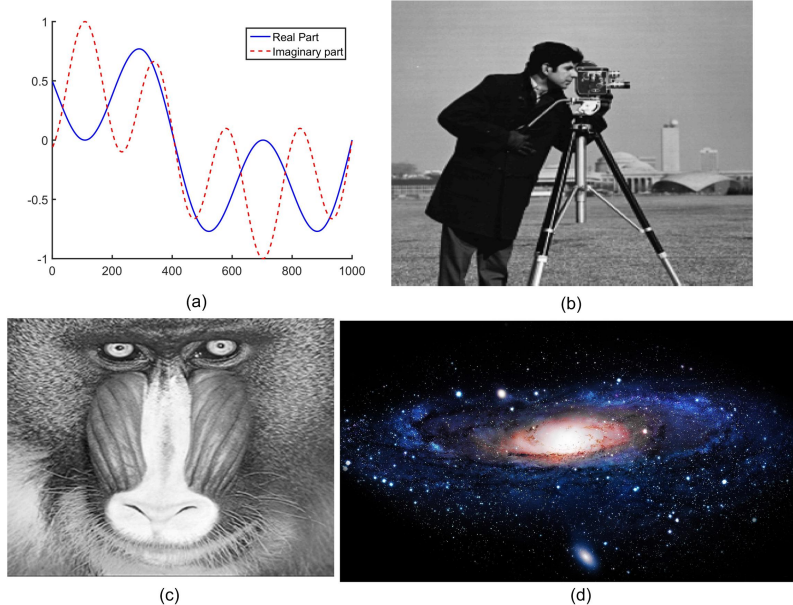


Fig. 1. Original signals: (a) Real and imaginary part of complex signal  $\mathbf{z}_{s1}$  with  $1000 \times 1$  pixels; (b) Amplitude and (c) phase part of complex image  $\mathbf{z}_{s2}$  with  $300 \times 300$  pixels<sup>1</sup>; (d) Natural image  $\mathbf{z}_{s3}$  with  $1080 \times 1920 \times 3$  pixels<sup>2</sup>.

The stepsize in FSAF method is chosen as the same as that used in modified Wirtinger flow (MWF) method [27] instead of an empirical value, which is one of the roots of the following univariate cubic equation of  $\alpha_k$ :

$$a_c \alpha_k^3 + b_c \alpha_k^2 + c_c \alpha_k + d_c = 0, \quad (8)$$

where various constant coefficients are given by  $a_c = \sum_{i=1}^m |h_i|^4$ ,  $b_c = -3 \sum_{i=1}^m \mu_i |h_i|^2$ ,  $c_c = \sum_{i=1}^m r_i |h_i|^2 + 2\mu_i^2$ , and  $d_c = -\sum_{i=1}^m u_i r_i$ . Here,  $h_i = \mathbf{a}_i^H \mathbf{v}_k$ ,  $\mu_i = \text{Re}((\mathbf{a}_i^H \mathbf{z}_k)^* h_i)$ , and  $r_i = |\mathbf{a}_i^H \mathbf{z}_k|^2 - y_i$  with “\*” denoting complex conjugate. A closed-form solution of cubic equation (8) can be easily calculated.

Finally, the complete implementation procedures of the proposed FSAF method are summarized as follows:

- Step 1) Initial step,  $k = 0$ ; Calculate the initial value  $\mathbf{c}_0$  based on the power iteration method and obtain  $\mathbf{z}_0 = \sqrt{t} \mathbf{F}_l \mathbf{c}_0$ .
- Step 2) Determine the search direction: Calculate truncated gradient of amplitude-based objective function  $\mathbf{d}_{tk}$  according to (6). Then determine the Polak-Ribière-Polyak (PRP) direction  $\mathbf{v}_k$  according to (7).
- Step 3) Determine the search length  $\alpha_k$  according to the roots in (8).
- Step 4) Update  $\mathbf{z}_{k+1} = \mathbf{z}_k - \alpha_k \mathbf{v}_k$ .
- Step 5) If the predefined termination condition (such as reaching a maximum iteration) is satisfied, stop the iteration. Otherwise, let  $k = k + 1$ , and go to step 2).

### 2.3. Computational complexity

For algorithms such as TWF, TAF, and STAF under Gaussian model, it requires at most  $O(\log(1/\epsilon))$  iterations to achieve  $\epsilon$ -accuracy with iteration cost  $O(mn)$  [18], [19], [20]. For the proposed method, the only difference with TAF in terms of computational complexity is that an additional FFT operation

<sup>1</sup> <https://homepages.cae.wisc.edu/ece533/images>

<sup>2</sup> Downloaded from <http://pics-about-space.com/milky-way-galaxy>.

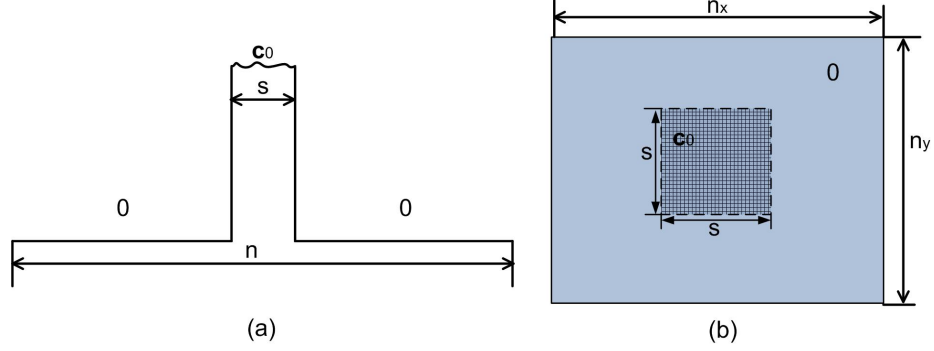


Fig. 2. Low-frequency coefficients  $c_0$  in FSI for 1D signal and 2D signal.

is added before two matrix-vector multiplications at the initial stage. The computational cost for the FFT operation is  $O(n \log(n))$ , which is much smaller than  $O(mn)$  considering  $n \leq m$ . Thus, the proposed method has the same computational cost with TAF.

### 3. Numerical Experiments

We present numerical experiments to illustrate the performance of the proposed FSAF algorithm. Both Gaussian and CDP models are considered. For the Gaussian model,  $\mathbf{a}_i \sim N(0, \mathbf{I}/2) + jN(0, \mathbf{I}/2)$ . For CDP models, we collect the data in the form of [18], [19]

$$\mathbf{y}^{(l)} = |\mathbf{F}\mathbf{D}^{(l)}\mathbf{z}|^2, \quad 1 \leq l \leq L, \quad (9)$$

which means that  $m = nl$ . Here,  $\mathbf{F}$  is the DFT matrix and  $\mathbf{D}^{(l)}$  is a diagonal matrix whose diagonal entries are randomly drawn from  $\{1, -1, j, -j\}$ , which models signal modulation before diffraction.

Two performance evaluation metrics were used: the first one is normalized mean square error (NMSE) as a function of number of iterations, where NMSE is calculated by

$$NMSE = \|\mathbf{z}_k - \mathbf{z}\|_F / \|\mathbf{z}\|_F, \quad (10)$$

where  $\mathbf{z}$  is the true signal, and  $\mathbf{z}_k$  is the signal recovered at the  $k$ th iteration. It should be noted that  $\mathbf{z}_k$  is multiplied by a constant value to get rid of the effect of a constant phase shift. The second one is empirical success rate among 100 independent runs with different random initials, in which success is declared when the returned NMSE is less than  $10^{-5}$  [16], [20].

Tests with noise models are also conducted. Specifically, we consider and discuss two noise models: The first one adds Gaussian noise by amplitude-type [19], [20], [28] with

$$\sqrt{\mathbf{y}} = |\mathbf{A}\mathbf{z} + \mathbf{n}_a|, \quad (11)$$

and the amplitude-based noise ratio  $R_a$  is quantified by  $R_a = (\|\mathbf{n}_a\|_F / \|\sqrt{\mathbf{y}}\|_F) \times 100\%$ . The second one adds Gaussian noise by intensity-type [18], [29] with

$$\mathbf{y} = |\mathbf{A}\mathbf{z}|^2 + \mathbf{n}_i \quad (12)$$

and the intensity-based noise ratio  $R_i$  is quantified by  $R_i = (\|\mathbf{n}_i\|_F / \|\mathbf{y}\|_F) \times 100\%$ .

As shown in Fig. 1, three complex signals including 1D signal, 2D image, and natural image are considered in this section. PR for 1D signals arises in various fields, such as fiber optics [30], speech recognition [31], and terahertz communications [32]. In coherent diffractive imaging [1], [2], [33] or Fourier ptychography [34], PR of 2D images and natural images also plays a crucial role. The first complex signal  $\mathbf{z}_{s1}$  shown in Fig. 1(a) is a combination of a few sinusoids with  $1000 \times 1$  pixels and represents a transfer function one might encounter in optics [15]. The 2D

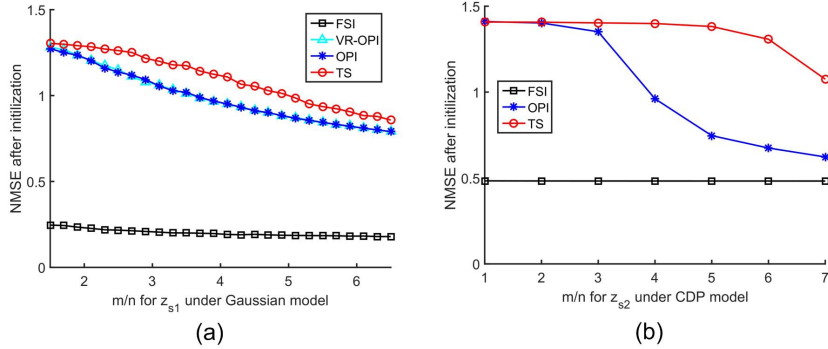


Fig. 3. The average NMSEs obtained from 100 independent trials with: frequency subspace initialization (FSI) proposed in this paper, variance-reducing orthogonality-promoting initialization (VR-OPI) in STAF [20], orthogonality-promoting initialization (OPI) in TAF [19], truncated spectral (TS) in TWF [18]. (a) Average NMSE after initialization for  $z_{s1}$  varying with sampling complexity  $m/n$  under Gaussian model; (b) Average NMSE after initialization for  $z_{s2}$  varying with sampling complexity  $m/n$  under CDP model.

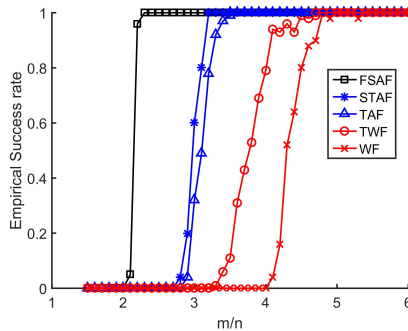


Fig. 4. Empirical probability of success based on 100 random trials for 1D complex signal  $z_{s1}$  under Gaussian model with a varied number of measurements.

complex signal  $z_{s2}$  tested under CDP model consists of the widely used “Cameraman” amplitude in Fig. 1(b) and “Baboon” phase in Fig. 1(c), where both amplitude and phase are with  $300 \times 300$  pixels. Finally, the natural image Milky Way Galaxy  $z_{s3}$  in Fig. 1(d) with  $1080 \times 1920 \times 3$  pixels is studied under CDP model, and results are compared with those reported in [16], [35], [19], [20].

### 3.1. Performance of Frequency Subspace Initialization

We study the performance of the proposed frequency subspace initialization (FSI) for recovering  $z_{s1}$  and  $z_{s2}$  under Gaussian and CDP models, respectively. As shown in Fig. 2, the high-frequency coefficients part of  $c_0$  are padded with zeros, where  $s$  is empirically chosen around 10 and 30 for 1D and 2D signals, respectively. Besides the proposed FSI, three other initialization schemes are also studied, including variance-reducing orthogonality-promoting initialization (VR-OPI) in STAF [20], orthogonality-promoting initialization (OPI) in TAF [19], truncated spectral (TS) in TWF [18]. For fair comparisons, all the parameters pertinent to implementation of each algorithm are set to their suggested values. The average NMSEs varying with sample complexity ( $m/n$ ) obtained from 100 independent trials using the four initialization schemes are presented in Fig. 3. Apparently, the proposed initialization method returns much more accurate and robust estimates than the existing methods in the literatures, where the returned NMSEs after initialization are 0.2 and 0.5

TABLE I  
COMPARISONS OF SAMPLE COMPLEXITY UNDER CDP MODEL FOR RECOVERING 2D COMPLEX IMAGE  $\mathbf{z}_{s2}$  AND NATURAL MILKY WAY GALAXY IMAGE  $\mathbf{z}_{s3}$ .

Algorithm	$L$ ( $\mathbf{z}_{s2}$ )	$L$ (reported for $\mathbf{z}_{s3}$ )
WF [16]	13	20 [16]
TWF [18]	7	6 [35]
TAF [19]	5	6 [19]
STAF [20]	NA <sup>1</sup>	8 [20]
The proposed FSAF method	3	3

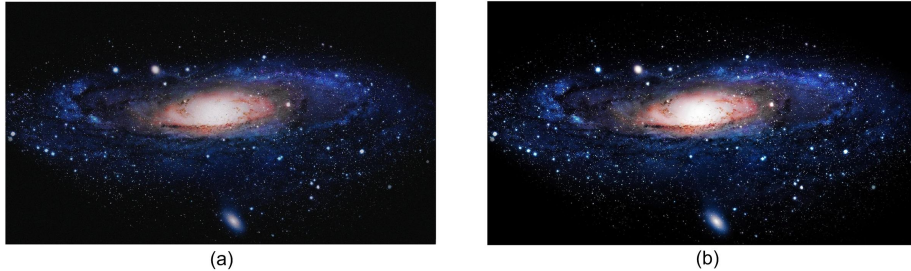


Fig. 5. Performance of the proposed FSAF algorithm on natural Milky Way Galaxy image  $\mathbf{z}_{s3}$  with  $1080 \times 1920 \times 3$  pixels for (a)  $L = 2$  masks and (b)  $L = 3$  random masks at the 150th iteration. For  $L = 2$  case, NMSEs after initialization and 150 iterations are 0.43 and 0.15, respectively. For  $L = 3$  case, NMSEs after initialization and 150 iterations are 0.43 and  $7.9e^{-16}$ , respectively.

in FSI for Gaussian and CDP models, respectively.

### 3.2. Phase Retrieval via Frequency Subspace Amplitude Flow

The second experiment evaluates performance of PR via the proposed FSAF method. Fig. 4 presents the empirical probability of success based on 100 random trials for 1D complex signal  $\mathbf{z}_{s1}$  under Gaussian model with a varied number of measurements. It shows that  $2.2n$  Gaussian phaseless measurements suffice for exact recovery ( $NMSE \leq 10^{-5}$ ) with high probability ( $\geq 95\%$ ) via the proposed FSAF approach. On contrary, it needs around  $3.2n$  and  $3.4n$  for exact recovery via STAF and TAF, respectively. For TWF and WF methods, around  $4.4n$  and  $4.7n$  phaseless measurements are needed, respectively. These results verify significant improvement of the proposed FSAF method on 1D complex signal.

We further test the method on various images with different sizes. Table I presents sample complexity ( $L$ ) under CDP model for recovering 2D complex image  $\mathbf{z}_{s2}$  and natural Milky Way Galaxy image  $\mathbf{z}_{s3}$ . To recover complex image  $\mathbf{z}_{s2}$ , 100 independent random trials with different initializations are conducted to compare the success rate of different algorithms. For an exact recovery ( $NMSE \leq 10^{-5}$ ) with high probability ( $\geq 95\%$ ), it needs only  $L = 3$  masks for the proposed method, which is much smaller than state-of-the-art, where  $L = 5$  masks are needed for TAF method. Fig. 5 presents the reconstructed results of the proposed FSAF algorithm on natural image Milky Way Galaxy  $\mathbf{z}_{s3}$  with  $1080 \times 1920 \times 3$  pixels for both  $L = 2$  and  $L = 3$  cases at the 150th iteration. Specifically, for  $L = 2$  case, NMSEs after initialization and 150 iterations are 0.43 and 0.15, respectively. For  $L = 3$  case, NMSEs after initialization and 150 iterations are 0.43 and  $7.9e^{-16}$ , respectively. It suggests that  $L = 3$  is sufficient for the proposed FSAF method to reconstruct Milky Way Galaxy image, which significantly outperforms the reported results in Table I when the same image is tested.

<sup>1</sup>There are no reported implementation details for recovering 2D complex image under CDP model for STAF, and we mark it as not applicable (NA) in order not to underestimate the method.

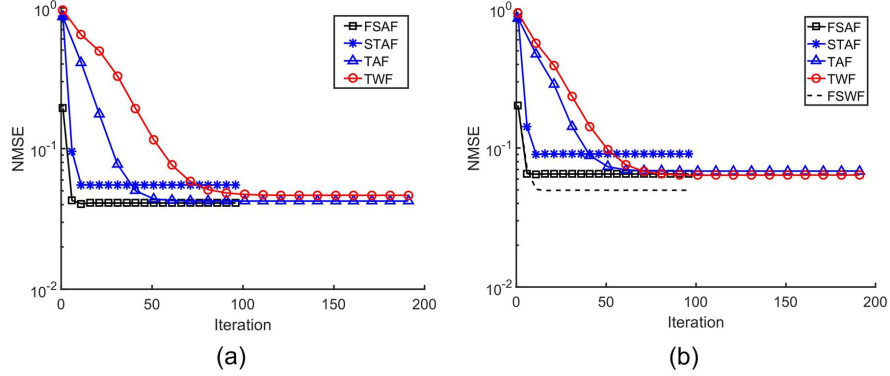


Fig. 6. NMSEs varying with iterations with  $m = 5n$  for reconstructing  $\mathbf{z}_{s1}$  with 5% (a) amplitude-type and (b) intensity-type Gaussian noise.

### 3.3. Noisy Measurements

The measurements contaminated by both amplitude-type and intensity-type Gaussian noises are also studied. Fig. 6(a) shows NMSEs varying with iterations for  $R_n = 5\%$  amplitude-type noise with  $m = 5n$  for reconstructing  $\mathbf{z}_{s1}$  under Gaussian models. The error curves show clearly that the proposed FSAF and STAF methods converge much faster than other methods. However, the final returned NMSE for STAF is apparently larger than other methods, and this phenomenon can also be observed in [20]. We repeat this experiment with intensity-type noise with  $R_n = 5\%$  in Fig. 6(b), and from all numerical simulations we have performed so far, we find that, the proposed FSAF method outperforms the other reported methods considering both convergence rate and accuracy.

More interesting, it is observed that the returned NMSEs for intensity-type noise in Fig. 6(b) are larger than those of amplitude-type noise in Fig. 6(a) for the proposed FSAF method. One reason is that amplitude-based gradient is used in the proposed FSAF method, and the objective function is different with the formulation of intensity-type noise. Since the proposed FSAF is highly flexible, we can simply replace the amplitude gradient  $\mathbf{d}_{tk}$  in FSAF by Wirtinger derivative [16]

$$\mathbf{d}_{wk} = \nabla f_1(\mathbf{z}_k) = \frac{1}{m} \sum_{i=1}^m (|\mathbf{a}_i^H \mathbf{z}_k|^2 - y_i) (\mathbf{a}_i \mathbf{a}_i^H) \mathbf{z}_k \quad (13)$$

with all other parameters and procedures unchanged. We mark the method as frequency subspace Wirtinger flow (FSWF). The FSWF method is found to be much more effective in dealing with intensity-type noise, which can be observed from the dashed NMSE curves in Fig. 6(b). Similar results have also been observed when  $\mathbf{z}_{s2}$  is reconstructed under CDP models.

It is noted that, although both the noisy models are widely used in literatures, it has at least been demonstrated in Fourier ptychography that amplitude-type noise model is more accurate than intensity-based model in practical situation [36]. Thus, the choice of gradient type plays a critical role in different situations, and a flexible algorithm such as FSAF is highly desirable.

## 4. Conclusions


This paper introduces a novel framework for PR, which has been shown to work very well in numerous tests. It pushes forward the state-of-the-art of sample complexity in PR of natural signals without increasing computational complexity. No additional constraint is needed in the proposed FSAF method, and it is applicable to natural images. Furthermore, from all numerical simulations we have performed so far, we find that, the proposed FSAF method outperforms the other reported methods considering both convergence rate and accuracy. Most importantly, the



results demonstrate that the proposed method is highly flexible, and can be easily adapted in both amplitude-type and intensity-type noise models.

## References

- [1] J. W. Miao, P. Charalambous, J. Kirz, and D. Sayre, "Extending the methodology of x-ray crystallography to allow imaging of micrometre-sized non-crystalline specimens," *Nature*, vol. 400, no. 6742, pp. 342–344, 1999.
- [2] K. A. Nugent, "Coherent methods in the x-ray sciences," *Advances in Physics*, vol. 59, no. 1, pp. 1–99, 2010.
- [3] D. Deng, W. Qu, W. He, Y. Wu, X. Liu, and X. Peng, "Phase retrieval for digital holographic microscopy with defocused holograms," *IEEE Photonics Journal*, vol. 10, no. 1, pp. 1–9, 2018.
- [4] W. Chen, "Single-shot imaging without reference wave using binary intensity pattern for optically-secured-based correlation," *IEEE Photonics Journal*, vol. 8, no. 1, pp. 1–9, 2016.
- [5] W. Chen, X. D. Chen, and C. J. R. Sheppard, "Optical image encryption based on diffractive imaging," *Optics Letters*, vol. 35, no. 22, pp. 3817–3819, 2010.
- [6] W. Chen, "Optical multiple-image encryption using three-dimensional space," *IEEE Photonics Journal*, vol. 8, no. 2, pp. 1–8, 2016.
- [7] R. W. Gerchberg, "A practical algorithm for the determination of the phase from image and diffraction plane pictures," *Optik*, vol. 35, pp. 237–246, 1972.
- [8] J. R. Fienup, "Phase retrieval algorithms - a comparison," *Applied Optics*, vol. 21, no. 15, pp. 2758–2769, 1982.
- [9] S. Marchesini, "Invited article: A unified evaluation of iterative projection algorithms for phase retrieval (vol 78, art no 011301, 2007)," *Review of Scientific Instruments*, vol. 78, no. 4, 2007.
- [10] H. H. Bauschke, P. L. Combettes, and D. R. Luke, "Hybrid projection-reflection method for phase retrieval," *Journal of the Optical Society of America a-Optics Image Science and Vision*, vol. 20, no. 6, pp. 1025–1034, 2003.
- [11] V. Elser, "Solution of the crystallographic phase problem by iterated projections," *Acta Crystallographica Section A*, vol. 59, pp. 201–209, 2003.
- [12] C. C. Chen, J. Miao, C. W. Wang, and T. K. Lee, "Application of optimization technique to noncrystalline x-ray diffraction microscopy: Guided hybrid input-output method," *Physical Review B*, vol. 76, no. 6, 2007.
- [13] L. J. Li, T. F. Liu, and M. J. Sun, "Phase retrieval utilizing particle swarm optimization," *IEEE Photonics Journal*, vol. 10, no. 1, pp. 1–9, 2018.
- [14] J. A. Rodriguez, R. Xu, C. C. Chen, Y. F. Zou, and J. W. Miao, "Oversampling smoothness: an effective algorithm for phase retrieval of noisy diffraction intensities," *Journal of Applied Crystallography*, vol. 46, pp. 312–318, 2013.
- [15] E. J. Candes, Y. C. Eldar, T. Strohmer, and V. Voroninski, "Phase retrieval via matrix completion," *Siam Review*, vol. 57, no. 2, pp. 225–251, 2015.
- [16] E. J. Candes, X. D. Li, and M. Soltanolkotabi, "Phase retrieval via wirtinger flow: Theory and algorithms," *IEEE Transactions on Information Theory*, vol. 61, no. 4, pp. 1985–2007, 2015.
- [17] Z. Wei, W. Chen, C.-W. Qiu, and X. Chen, "Conjugate gradient method for phase retrieval based on the wirtinger derivative," *Journal of the Optical Society of America A*, vol. 34, no. 5, pp. 708–712, 2017.
- [18] Y. Chen and E. Candes, "Solving random quadratic systems of equations is nearly as easy as solving linear systems," in *Advances in Neural Information Processing Systems*, 2015, pp. 739–747.
- [19] G. Wang, G. B. Giannakis, and Y. C. Eldar, "Solving systems of random quadratic equations via truncated amplitude flow," *arXiv preprint arXiv:1605.08285*, 2016.
- [20] G. Wang, G. B. Giannakis, and J. Chen, "Scalable solvers of random quadratic equations via stochastic truncated amplitude flow," *IEEE Transactions on Signal Processing*, vol. 65, no. 8, pp. 1961–1974, 2017.
- [21] Z. Wei, W. Chen, T. Yin, and X. Chen, "Robust phase retrieval of complex-valued object in phase modulation by hybrid wirtinger flow method," *Optical Engineering*, vol. 56, no. 9, p. 093106, 2017.
- [22] Y. Shechtman, A. Beck, and Y. C. Eldar, "Gespars: Efficient phase retrieval of sparse signals," *IEEE Transactions on Signal Processing*, vol. 62, no. 4, pp. 928–938, 2014.
- [23] P. Schniter and S. Rangan, "Compressive phase retrieval via generalized approximate message passing," *IEEE Transactions on Signal Processing*, vol. 63, no. 4, pp. 1043–1055, 2015.
- [24] D. S. Taubman and M. W. Marcellin, *JPEG2000 Image Compression Fundamentals, Standards and Practice*, 1st ed. Boston, MA: Springer US, 2002, vol. 642.
- [25] E. Polak and G. Ribiere, "Note sur la convergence de methodes de directions conjuguées," *Revue française d'informatique et de recherche opérationnelle. Serie rouge*, vol. 3, no. 16, pp. 35–43, 1969.
- [26] X. D. Chen, "Subspace-based optimization method for solving inverse-scattering problems," *IEEE Transactions on Geoscience and Remote Sensing*, vol. 48, no. 1, pp. 42–49, 2010.
- [27] X. Jiang, S. Rajan, and X. Z. Liu, "Wirtinger flow method with optimal stepsize for phase retrieval," *IEEE Signal Processing Letters*, vol. 23, no. 11, pp. 1627–1631, 2016.
- [28] P. Netrapalli, P. Jain, and S. Sanghavi, "Phase retrieval using alternating minimization," *IEEE Transactions on Signal Processing*, vol. 63, no. 18, pp. 4814–4826, 2015.
- [29] N. Vaswani, S. Nayer, and Y. C. Eldar, "Low-rank phase retrieval," *IEEE Transactions on Signal Processing*, vol. 65, no. 15, pp. 4059–4074, 2017.
- [30] A. Carballar and M. A. Muriel, "Phase reconstruction from reflectivity in fiber bragg gratings," *Journal of lightwave technology*, vol. 15, no. 8, pp. 1314–1322, 1997.
- [31] L. Rabiner and B. H. Juang, *Fundamentals of speech recognition*. PTR Prentice Hall, 1993.
- [32] T. Kleine-Ostmann and T. Nagatsuma, "A review on terahertz communications research," *Journal of Infrared, Millimeter, and Terahertz Waves*, vol. 32, no. 2, pp. 143–171, 2011.

- 
- [33] J. Bertolotti, E. G. van Putten, C. Blum, A. Lagendijk, W. L. Vos, and A. P. Mosk, "Non-invasive imaging through opaque scattering layers," *Nature*, vol. 491, no. 7423, pp. 232–234, 2012.
  - [34] G. Zheng, R. Horstmeyer, and C. Yang, "Wide-field, high-resolution fourier ptychographic microscopy," *Nat Photon*, vol. 7, no. 9, pp. 739–745, 2013.
  - [35] H. Zhang, Y. Zhou, Y. Liang, and Y. Chi, "Reshaped wirtinger flow and incremental algorithm for solving quadratic system of equations," *arXiv preprint arXiv:1605.07719*, 2016.
  - [36] L.-H. Yeh, J. Dong, J. Zhong, L. Tian, M. Chen, G. Tang, M. Soltanolkotabi, and L. Waller, "Experimental robustness of fourier ptychography phase retrieval algorithms," *Optics Express*, vol. 23, no. 26, pp. 33 214–33 240, 2015.
- 